

RESEARCH ARTICLE

Sensory Processing

How does orientation-tuned normalization spread across the visual field?

✉ Michaela Klímová,^{1,2,3} Ilona M. Bloem,⁴ and Sam Ling^{1,2}¹Department of Psychological and Brain Sciences, Boston University, Boston, Massachusetts, United States; ²Center for Systems Neuroscience, Boston University, Boston, Massachusetts, United States; ³Department of Psychology, Northeastern University, Boston, Massachusetts, United States; and ⁴Computational Cognitive Neuroscience and Neuroimaging, Netherlands Institute for Neuroscience, Amsterdam, The Netherlands

Abstract

Visuocortical responses are regulated by gain control mechanisms, giving rise to fundamental neural and perceptual phenomena such as surround suppression. Suppression strength, determined by the composition and relative properties of stimuli, controls the strength of neural responses in early visual cortex, and in turn, the subjective salience of the visual stimulus. Notably, suppression strength is modulated by feature similarity; for instance, responses to a center-surround stimulus in which the components are collinear to each other are weaker than when they are orthogonal. However, this feature-tuned aspect of normalization, and how it may affect the gain of responses, has been understudied. Here, we examine the contribution of the tuned component of suppression to contrast response modulations across the visual field. To do so, we used functional magnetic resonance imaging (fMRI) to measure contrast response functions (CRFs) in early visual cortex (areas V1–V3) in 10 observers while they viewed full-field center-surround gratings. The center stimulus varied in contrast between 2.67% and 96% and was surrounded by a collinear or orthogonal surround at full contrast. We found substantially stronger suppression of responses when the surround was parallel to the center, manifesting as shifts in the population CRF. The magnitude of the CRF shift was strongly dependent on voxel spatial preference and seen primarily in voxels whose receptive field spatial preference corresponds to the area straddling the center-surround boundary in our display, with little-to-no modulation elsewhere.

NEW & NOTEWORTHY Visuocortical responses are underpinned by gain control mechanisms. In surround suppression, it has been shown that suppression strength is affected by the orientation similarity between the center and surround stimuli. In this study, we examine the impact of orientation-tuned suppression on population contrast responses in early visual cortex and its spread across the visual field. Results show stronger suppression in parallel stimulus configurations, with suppression largely isolated to voxels near the center-surround boundary.

contrast response functions; divisive normalization; fMRI; surround suppression; vision

INTRODUCTION

Visual perception is heavily influenced by context—a principle exemplified by the perceptual phenomenon known as surround suppression. Under surround suppression, the perceived contrast of a stimulus is attenuated in the presence of a surrounding stimulus (1–3). Surround suppression's neural underpinnings are typically observed in animal electrophysiological recordings as decreases in central receptive field (RF) responses when an annulus is placed within its extraclassical surround (4–10).

Although the addition of a surround stimulus is typically suppressive (5, 6, 8–11), the specific properties of the center and surround stimuli dictate the degree to which suppression will occur (12, 13). Specifically, suppression strength appears to be governed by the relative feature similarity between the two components, with the strongest suppression occurring when the surround and central stimuli are matched in orientation and spatial frequency (5, 10, 14–18). This feature-tuned component of suppression has been proposed to serve a number of functional roles in cortex, such as facilitating the use of spatial context to parse visual scenes,



Correspondence: M. Klímová (m.klimova@northeastern.edu).

Submitted 29 May 2024 / Revised 13 December 2024 / Accepted 27 December 2024





supporting redundancy reduction and efficient neural coding (12, 19).

Computationally, the influence of the surround on the center is well accounted for as a form of divisive modulation (5, 20–22), in which the excitatory drive from the center stimulus is divided by a proportional suppressive drive, composed of a more broadly spatially tuned pool of units responding to both the center and the surrounding region of space. Divisive normalization (20, 23) has been put forth as a putative canonical computation, providing an explanatory account of a variety of nonlinear behaviors observed within visuocortical neurons, including surround suppression (20).

Another key feature of normalization models is their ability to describe the nonlinear relationship between a stimulus's contrast and its subsequent neural response (4, 20)—a relationship commonly referred to as the contrast response function (CRF) (24, 25). Although surround suppression has long been characterized as a signature of normalization, neuroimaging studies have been hindered by a lack of proper quantification of suppressive effects on the contrast response (26, 27), both within and across early visual areas. Although previous neuroimaging work from our laboratory and others has consistently found suppression of responses when pairs of stimuli are aligned in a collinear configuration, compared with orthogonal (14, 15, 28–31), it is still unclear how surround suppression interacts with the population-level CRF.

In this study, we sought to identify changes in the gain underlying orientation-tuned suppression, both within and across early visual cortices. To do so, we presented participants with center-surround stimuli and measured changes in BOLD response as we parametrically varied the contrast of the center. Specifically, we varied the contrast of a central grating stimulus at nine contrast levels, while the center was surrounded by a large, full contrast annulus grating that was either collinear or orthogonal in its orientation content relative to the center stimulus. We found that the contrast response functions of voxels with population receptive fields far from the center-surround boundary were not influenced by the orientation of the surround. However, the contrast response of voxels that were spatially selective to the center-surround boundary exhibited a gain shift to the collinear surround, relative to orthogonal. These results suggest that the effects of tuned normalization on the gain of responses within human visual cortex are spatially local to the areas of competition, rather than across the entire center stimulus representation.

METHODS

Observers

Ten observers (8 female) took part in the experiment. All were between the ages of 18 and 35 and reported normal or corrected-to-normal visual acuity. All participants gave their written informed consent, and the study was approved by the Boston University Institutional Review Board. Observers received monetary compensation for their participation, except one (one of the authors of the study).

Apparatus and Stimuli

Stimuli were programmed and rendered on a MacBook Pro (OS X 10.7) using MATLAB (2015 b; MathWorks, Natick,

MA) and Psychophysics Toolbox (Brainard, 1997). The stimuli were displayed on a rear-projection screen in the scanner bore, using a gamma-corrected projector (ProPixx DLP LED, VPixx Technologies; max. luminance 306 cd/m²) and observers viewed them via a front-surface mirror affixed to the head coil. Participants were provided with a two-button box for behavioral responses.

The visual stimulus was a 2 cycles/deg (cpd) center grating (inner radius 0.75 dva from central fixation, outer radius 2.95 dva), which varied in contrast throughout each fMRI run, surrounded by a 2 cpd annular grating (inner radius 3.05 dva, outer radius 8.5 dva), with a 0.1 dva gap between the central and surround component (Fig. 1A). The small gap was chosen based on prior work that found strongest center-surround interactions with minimal spatial separation between the two components (1, 32–34). Prior work also informed the eccentric location of the center-surround boundary; surround suppression tends to be stronger when stimuli are presented away from fovea (2). Both gratings were embedded in a Gaussian envelope. The contrast of the center grating varied over nine logarithmically spaced contrast levels (2.67%, 4.0%, 5.33%, 8.0%, 16%, 32%, 48%, 64%, and 96% Michelson contrast), while the surround grating contrast was always 100% Michelson contrast. Both gratings had their spatial phase updated every 100 ms to a randomly chosen value, independently of each other. The surround grating could either be collinear or orthogonal with respect to the center. The central grating orientation remained identical throughout each run and was either 45° or 135° in alternating runs, with starting orientation counterbalanced between observers. Stimuli were presented on a mean luminance background.

MRI Data Acquisition

All MRI data were collected at the Center for Cognitive Neuroimaging center at Boston University on a Siemens 3 T Prisma scanner with a 64-channel head coil, in a single 2-h session. fMRI data were acquired with simultaneous multi-slice (multiband acceleration factor 5) echoplanar T2*-weighted sequence (voxel size 2 mm³, TR = 1,000 ms, TE = 30 ms, echo spacing = 0.67 ms, flip angle = 64°, FOV = 208 × 208 × 140 mm). Before this session, each participant also went through a separate population receptive field (pRF) mapping session using the same T2*-weighted protocol, in addition to a high-resolution anatomical scan (T1-weighted multiecho MPRAGE sequence, FOV = 256 × 256 × 176 mm, 36 slices, TR = 2530 ms, TE = 1.69 ms, FA = 7°, voxel size = 1 mm³).

Experimental Procedure

Main task.

The main task had 498 TRs (1 s TR), and most participants completed 10 runs (one completed 8, and two completed 9). Stimuli were presented in an event-related design, with 4 s event duration and jittered intertrial interval between 6 and 17 s. The event schedules were generated using the FreeSurfer tool Optseq2 (35). To promote nonlinear contrast response functions, we used a contrast adaptation paradigm previously established in our laboratory (27, 36). Following a 4-s baseline period with a mean luminance screen, the phase-jittered central grating was presented for 60 s at 16% contrast

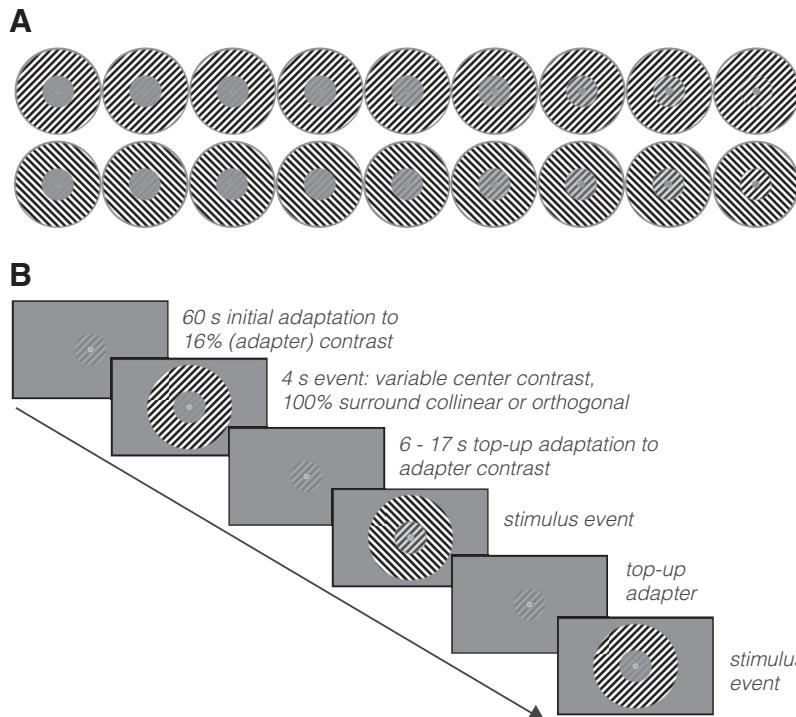


Figure 1. *A:* experimental stimuli. Center contrast increases from left to right. *Top row:* collinear surround, *bottom row:* orthogonal surround. *B:* three example trials occurring at the start of a scan. Following the 60 s adaptation period, trial order is pseudorandomized, and intertrial intervals serve as top-up adapters to the 16% adapter contrast. In this example, the center grating orientation is 45°. Note that spatial frequency was lowered for illustration purposes.

(adapting contrast) in an initial adaptation block. Following this initial adaptation, the event-related stimulus presentation began. During the stimulus event, the center grating changed contrast to the target contrast for that event and was surrounded by either a collinear or orthogonal 100% contrast grating. The intertrial intervals served as top-up adaptation periods, during which the center grating again changed contrast to the adapting contrast intensity. An example stimulus sequence is depicted in Fig. 1*B*. Each of the nine center contrast levels (including the adapting contrast) was presented four times within an fMRI run, twice with a collinear surround and twice with an orthogonal surround. We followed the contrast adaptation paradigm introduced by Vinke et al. (27), which was designed to bring out the compressive nonlinearity in population CRFs. Typically, BOLD responses in fMRI are found to scale linearly with increasing contrast (37), diverging from results established in individual visuocortical neurons, which exhibit saturation near high contrasts. This is likely due to each voxel containing a large neural population with variable CRFs. Adaptation is known to bring the most sensitive portion of the CRF toward the adapting contrast (38); therefore, adapting the population to a single low contrast level should reduce neural variability within each voxel, making it possible to detect nonlinearities in the population CRF (26, 27).

Participants were engaged in a rapid letter detection and identification task at fixation. The small (0.1 dva) fixation dot in the center of the screen was red and surrounded by a white circular 1.5 dva diameter annulus. White letters were displayed within this annulus, in front of the fixation point, continuously throughout the run. Participants' task was to monitor this letter stream for letters "J" and "K" amid 10 other distractor letters ("X," "L," "V," "H," "S," "A," "C," "P," "Z," and "Y"). A new letter was presented every 200 ms, and participants were asked to press the left button on the

response box as soon as they detected "J" and the right button for "K." At the end of each run, performance accuracy was displayed to the participants for feedback. Accuracy across participants was 90.2% on average ($\pm 2.4\%$ SE).

Functional localizer.

Each session began with two runs of a functional localizer, intended to isolate voxels responding to the center and the surround stimulus areas of the visual field. The localizer had a stimulus on (16 s)-stimulus off (16 s) blocked design, with 208 TRs (1 s TR), with each scan beginning and ending with an off block. The localizer stimulus was a 100% Michelson contrast, achromatic checkerboard (fundamental frequency: 2 cpd) with the same inner and outer diameter as the main stimulus, on a mean luminance background, and the behavioral task was identical to the main experiment. Following the localizer runs, participants began the main task.

Population receptive field mapping session.

For each observer, pRF mapping was carried out in a separate session, using stimuli and analysis code from the analyzePRF toolbox (39). In a single session, each observer underwent 10 pRF mapping runs (300 TRs, 1 s TR), which alternated five sweeping bar stimulus runs and five runs with a combination of rotating wedge and expanding and contracting ring. The results of analyzePRF were used to manually draw cortical surface labels outlining early visual areas V1, V2, and V3, by identifying polar angle preference reversals. The early visual area labels then served as a tool in voxel selection for functional data analysis.

MRI Data Analyses

Anatomical data.

The 1 mm³ T1 images acquired during the pRF mapping session were analyzed in FreeSurfer using the recon-all

pipeline. The results were used to register the functional data to the anatomical data.

fMRI preprocessing and beta weight estimation.

Reverse-phase encoding (40) was used to correct EPI distortion in the functional data in FSL (41). Following distortion correction, data were preprocessed with FS-FAST (42) with no spatial smoothing ($\text{FWHM} = 0 \text{ mm}$), implementing standard motion correction, Siemens slice timing correction, and boundary-based registration (43). We used robust rigid registration (44) to achieve accurate voxel-to-voxel correspondence between functional runs within a session, aligning the middle TR of each run to the middle TR of the first run of the session. To identify voxels responsive to the stimuli, the functional localizer data for each localizer type (center and surround) were analyzed in FreeSurfer with a GLM analysis following robust registration. The main task data were further processed using custom MATLAB scripts. We extracted voxels that fell within the pRF labels V1, V2, and V3. Following the removal of the beginning 64 TRs from each run (the 4 s initial baseline + the 60 s initial adaptation period), the time series data were low-pass filtered (filter cutoff 0.01 Hz), converted to % signal change by dividing the BOLD signal at each time point by the average BOLD signal value of the run and concatenated.

We constrained our voxel inclusion as follows: first, we selected only voxels responding to either the center or surround localizer, defined as a GLM P value of 0.05 or less. Out of these voxels, we further selected only those with a pRF variance explained (R^2) of 0.1 or above, and those whose eccentricity estimates fell within the stimulus bounds (i.e., between 0.75 and 8.5 dva). Furthermore, we ensured that voxels whose region of interest label overlapped were removed to avoid the inclusion of duplicate voxels in the dataset. After the application of these criteria, we had on average 719 ± 174 (SD) voxels in V1, 485 ± 88 voxels in V2, and 335 ± 42 voxels in V3.

Contrast response estimation.

After finalizing the initial voxel selection, we implemented a voxel-wise finite impulse response (FIR) analysis (35) in MATLAB. This method estimates the shape of the BOLD response to each stimulus type without assumptions about the underlying hemodynamic response function. The full-time course of each stimulus type (i.e., each combination of contrast level and surround orientation) was modeled with 20 regressors. The analysis resulted in 20 beta weight estimates for each condition. Finally, we computed the mean beta weight in each condition within an averaging window of 4–8 TRs after stimulus onset, accounting for the hemodynamic response delay and capturing the peak of the hemodynamic response function for each observer and condition, resulting in a voxel-wise contrast response function of 9 points (contrast levels) per condition.

Contrast response function model fitting.

The contrast response function for voxels within the center grating stimulus dimensions (between 0.75 and 2.95 dva) was fit with a variant of the Naka-Rushton equation (24, 25):

$$R(c) = R_{\max} \frac{c^n}{c^n + C_{50}^{-n}} + b$$

Here, the BOLD response (R) at each contrast level (c) is determined by the maximum attainable response (R_{\max}), the contrast at the semisaturation point (the semisaturation constant, C_{50}), an exponent (n), and an additive baseline parameter (b). MATLAB's *fmincon* function was used to implement the fit by minimizing the sum of squared errors (SSE) between the Naka-Rushton model and the measured CRF for each voxel. We constrained the R_{\max} parameter to be between 0 and 10 (beta weight, or % signal change) and the C_{50} parameter to be between 1 and 80 (% contrast). The baseline parameter was fixed per voxel to the average of the voxel's responses to the lowest contrast between the collinear and the orthogonal surround condition. Furthermore, we did not anticipate significant changes in the n parameter based on existing literature (4–6, 10); therefore, we opted to fix the value of n to 2 in each voxel (20, 45). The fitting procedure converged on a solution for all voxels. A goodness-of-fit estimate was obtained by computing the R^2 of the Naka-Rushton fit for each voxel. Model fitting was conducted in MATLAB, while most statistical tests were performed in R. We only fit the Naka-Rushton to the voxels corresponding to the center stimulus, as the surround voxel response was not expected to vary as a function of the center stimulus contrast (see Fig. 2).

Eye Position Monitoring

Throughout the experimental session, participants' gaze was monitored using an MR-compatible eye-tracking setup (EyeLink 1000, SR Research, Ontario, Canada) with a sampling rate of 1,000 Hz (3 observers) or 500 Hz (7 observers). After excluding blinks, the average eye deviation from the fixation point in the center of the screen across participants was 0.21 ± 0.09 dva SE in horizontally and 0.2 ± 0.11 dva SE vertically. This is well within the bounds of the fixation circle, whose radius was 0.75 dva. Therefore, participants maintained reliable fixation throughout the experimental session.

RESULTS

Contrast Response Functions under Orientation-Tuned Suppression

Given the spatial layout of our full-field stimulus, we reasoned that any orientation-tuned modulation would be most apparent for voxels whose pRF location (eccentricity) is near the center-surround boundary. Instead of averaging the voxel-wise CRFs across the whole ROI, we binned the voxels into 8 bins based on their pRF-preferred eccentricity. We first divided the stimulus into two portions: center (between 0.75 and 3.05 dva radius) and surround (between 3.05 and 8.5 dva radius), with the inner radius of the surround stimulus serving as the dividing line. We then divided each half of the display into four equal-sized eccentricity bins. As depicted in Fig. 2, in the bin closest to fixation, the contrast responses to the collinear and orthogonal-flanked condition largely overlap. The responses begin to diverge as a function of distance to the center-surround boundary, with the strongest suppression of the collinear responses in the fourth

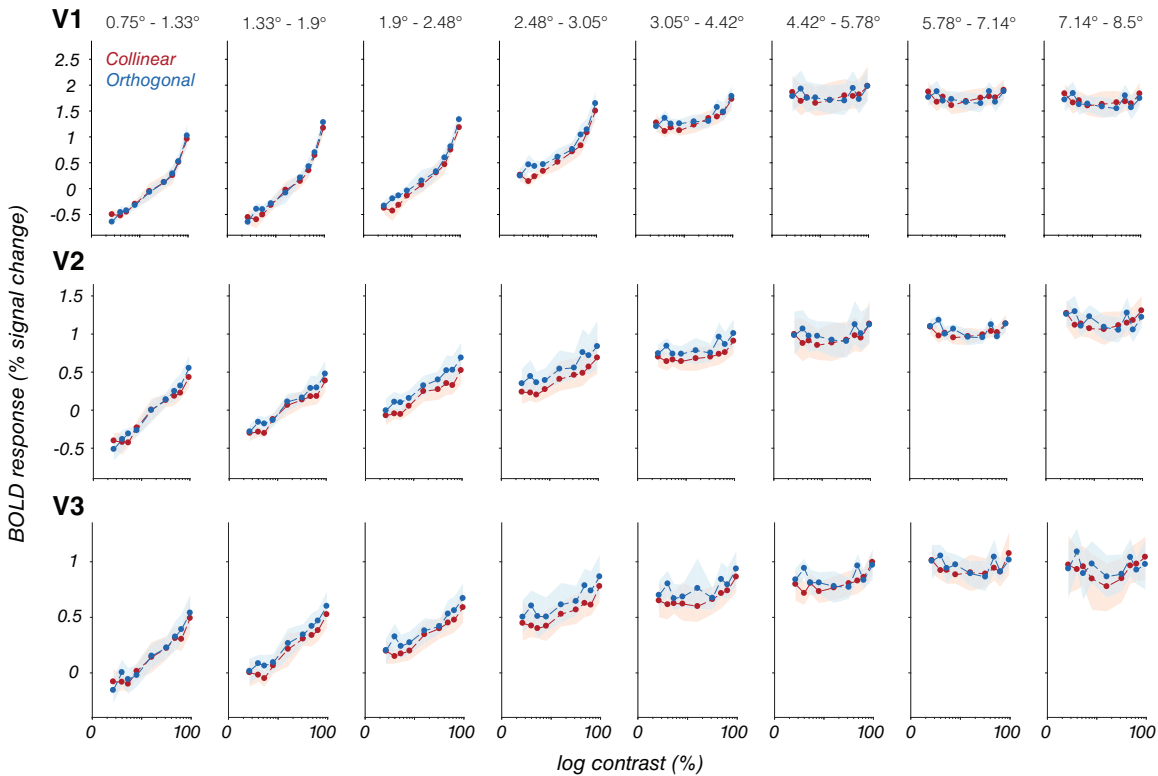


Figure 2. Averaged eccentricity-binned contrast responses. Each plot depicts the BOLD response as a function of center contrast (log-scaled). Center contrast values were 2.67%, 4%, 5.33%, 8%, 16% (adapter contrast), 32%, 48%, 64%, and 96%. Each row summarizes results from one visual area; V1: upper row, V2: middle row, V3: bottom row. Left four columns represent the four eccentricity bins into which the center stimulus was divided, right four columns show the four bins of the surround annulus. The bounds of each eccentricity bin are listed above the columns. Center-surround boundary is located at 3.05° from fixation. The plots were obtained by averaging the % signal change across all voxels per observer ($n = 10$) in each bin, and then computing between-observer averages in each condition for that bin (red: collinear, blue: orthogonal). Error bars represent ± 1 SE.

bin (the center stimulus band abutting the surround). Small differences between collinear and orthogonal conditions persist in the first surround bin, and as expected, the outermost bins show largely flat responses for both conditions (due to the contrast of the surround remaining fixed at 100% contrast), which again largely overlap.

Orientation-Tuned Suppression across the Visual Field

To quantify the relationship between suppressive gain modulation for the collinear surround with voxel position relative to the center-surround boundary, we computed the average overall tuned suppression strength in each eccentricity bin. First, we averaged the voxel-wise % signal change across contrast levels. Overall suppression was computed by subtracting the % signal change in the collinear-surround condition from the orthogonal-surround condition. Observer-averaged gain modulation as a function of voxel placement within the stimulus is depicted in Fig. 3. Suppression in the center stimulus (first four bins) gradually increased across eccentricity and reached a maximum in the center stimulus band that neighbored the surround. A mixed linear model (observers as random effects, absolute distance from the boundary and ROI as fixed effects) including all voxels in our sample revealed that the absolute distance from the center-surround boundary at 3.05° (in dva) significantly predicted orientation-tuned suppression strength $\{\beta = -0.03, 95\% \text{ CI} [-0.03, -0.03], t(153,874) = -79.91, P < 0.001\}$, confirming

that the differences in % signal change were largest near the center-surround boundary. The effects of ROI were also significant; compared with V1, tuned normalization effects (% signal change differences between collinear and orthogonal surround) were more pronounced in V2 $\{\beta = 0.03, 95\% \text{ CI} [0.03, 0.03], t(153,874) = 27.59, P < 0.001\}$ and V3 $\{\beta = 0.008, 95\% \text{ CI} [-0.0065, 0.01], t(153,874) = 6.98, P < 0.001\}$.

Quantifying Contrast Response Function Modulations

The variability of voxel-wise CRFs, and hence, that of Naka-Rushton parameters, was substantial in all three visual areas. Although most voxels had nonlinear CRFs, many CRFs did not saturate at high contrasts, likely due to stimulus optimality issues (see DISCUSSION). We therefore include the Naka-Rushton comparison as an exploratory analysis of the nature of CRF gain modulation across voxels. To compare the voxel-wise CRF parameters between the two surround configurations, we selected center stimulus voxels based on 1) whether the extent of their pRFs included the boundary between the center and the surround and 2) Naka-Rushton goodness-of-fit. For each voxel, we added and subtracted the pRF size estimate to/from the voxel's pRF eccentricity estimate, to obtain approximate coverage of the pRF within the stimulus. From this narrowed selection, we excluded voxels whose Naka-Rushton R^2 was below 0, leading us to drop 21.3% voxels from V1, 51.4% in V2, and 50.3% in V3. Across participants, on average 59 (± 24 SD) voxels in

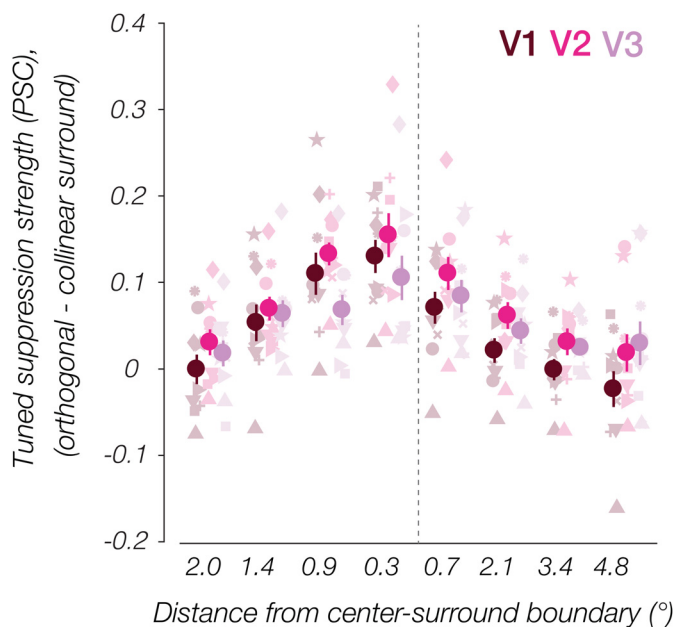


Figure 3. Tuned suppression as a function of voxel position within the center-surround stimulus. First, the voxel-wise average BOLD response across all contrast levels was computed in each stimulus eccentricity bin in both conditions (collinear vs. orthogonal surround). We subsequently subtracted the averaged BOLD response in the collinear surround condition from the orthogonal surround BOLD response for each participant and averaged across participants ($n = 10$) in each bin. The leftmost data points represent the eccentricity bin closest to fixation. The center-surround boundary (3.05°) is between the fourth (outermost center) and fifth bin (innermost surround) and is represented by the gray dashed line. Error bars represent ± 1 SE (PSC = % signal change).

V1, 25 (± 12) voxels in V2, and 19 (± 8) voxels in V3 fulfilled this criterion. The average eccentricity of the center of the voxels' pRF was 2.7° from fixation across ROIs ($\pm 0.3^\circ$ SD). In this subset, we compared collinear versus orthogonal median C_{50} and R_{\max} estimates in each ROI using a one-sided pairwise Wilcoxon test [reflecting our reasoning that if suppression is stronger in the collinear configuration, consistent with psychophysical findings (1, 2), we expect to find a higher C_{50} in this condition, and/or a lower R_{\max} , as seen in electrophysiology] (5). C_{50} was overall higher in the collinear condition (in V1, the average of median C_{50} values was $50\% \pm 7\%$ in the collinear condition and $37\% \pm 6\%$ in the orthogonal condition). In V2, collinear C_{50} was $20.5\% \pm 4\%$ and orthogonal C_{50} was $11.6\% \pm 2.5\%$. In V3, collinear C_{50} was $37\% \pm 8\%$, while orthogonal was $26\% \pm 7.4\%$. However, this difference did not reach statistical significance in any ROI. Likewise, R_{\max} (V1: collinear R_{\max} was $1.46 \pm 0.08\%$ signal change, orthogonal 1.5 ± 0.1 ; V2: collinear R_{\max} 0.6 ± 0.1 , orthogonal 0.8 ± 0.2 ; V3: collinear 0.5 ± 0.06 , orthogonal 0.6 ± 0.05) did not differ between conditions in any ROI.

DISCUSSION

We investigated how orientation-tuned suppression modulates the gain of visuocortical contrast responses, by measuring early visual BOLD signal modulations to a contrast-varying center grating surrounded by a full contrast annulus either collinear or orthogonal to the center. We found suppressive gain modulation in the collinear surround configuration

compared with orthogonal, with lower BOLD responses and population CRF shifts relative to orthogonal. Extrastriate cortex generally showed stronger suppression by parallel surround relative to orthogonal, compared with V1. Orientation-dependent CRF shifts were observed predominantly in voxels whose pRF location and size positioned them such that they received stimulation from both center and surround stimuli and were maximal in center voxels directly bordering the surround annulus. Near-foveal voxels instead showed a strong overlap between the collinear and orthogonal CRFs. This pattern suggests that orientation-tuned suppression from the surround is spatially local, as opposed to spreading to the entire center stimulus.

Broadly, our findings are in agreement with prior fMRI studies in early visual areas demonstrating the orientation dependency of surround suppression, in which parallel surrounds induced stronger BOLD signal suppression compared with orthogonal surrounds (14, 15, 18, 29, 31). Past fMRI results complement psychophysical studies of surround suppression, in which the apparent contrast of a central stimulus is lower in the presence of a high-contrast surround (1–3, 46), and this suppressive effect is stronger with collinear surrounds as compared with orthogonal (1, 2, 46). When it comes to breaking down the surround suppression effects across the visual field, to our knowledge, there is limited work directly examining how magnitude of perceptual suppression might vary across the center in a center-surround stimulus, and instead, it is largely assumed the perceived contrast of the center stimulus (and the underlying neural response) is constant across its area. A recent fMRI study (47) compared BOLD responses to a center-surround stimulus with either a large grating, a congruent figure-ground grating (same orientation, but with a small gap), and incongruent figure-ground grating (orthogonal orientations and small gap) and found that the differential responses of V1 voxels to the congruent versus incongruent stimuli were detectable even in the innermost band of the center stimulus, unlike in the present findings. However, the experiments are not directly comparable as we did not have a no-gap condition, and the center figure was only 4° in diameter, compared with our 6° . On the other hand, psychophysical results (48) suggest that when the innermost portion of a central grating in a center-surround stimulus is removed, thus forcing participants to use the edge of the center abutting the surround for contrast detection, thresholds increased similarly to a regular center-surround configuration, suggesting that the effect of a high-contrast surround stimulus extends slightly beyond its area. Our participants did not indicate any differences in perceptual suppression strength between the innermost areas of the center stimulus and those closer to the surround annulus. Future work could address whether there are psychophysical differences in suppression strength as a function of distance from the suppressing stimulus, or whether there is a perceptual filling-in effect at play which is not reflected in the early visual BOLD responses.

Mirroring prior electrophysiological work, we see considerable variability among individual CRF measurements (4–6, 8–10, 49). In electrophysiology, neuronal CRFs are fit with the Naka-Rushton equation, a variant of the normalization model. The two most observed CRF modulations as a result of placement of a suppressive surround are contrast gain (a rightward shift of the CRF and a corresponding increase in

the semisaturation constant) and response gain (compression of the CRF at high contrasts, and a decrease in the maximum response). Contrast gain is thought to bring the most sensitive portion of the CRF toward the ambient contrast level (38), thereby optimizing the sensitivity of the neuron through divisive computations, while response gain decreases responsiveness at higher contrasts. Prior studies mostly report a mixture of effects (5, 8), and more recent evidence has suggested that the type of modulation may be determined by the spatial frequency preference of the cell (50). In the current dataset, lack of CRF saturation in many voxels limits our ability to conclusively comment on the exact nature of voxel-wise gain modulation, although exploratory analyses indicate an increase in the semisaturation constant in the collinear condition relative to orthogonal.

The lower rate of saturation in our data diverges somewhat from other fMRI studies using adaptation to recover saturating nonlinearities in the population CRF (27, 36). We suspect nonsaturation in our data was caused by the relative lack of stimulus optimality for early visual cortex; specifically, we did not account for cortical magnification in the stimulus spatial frequency, which was done by Vinke et al. (27), and the center grating stimulus was not oriented radially from fixation, as done in Vinke et al. (27), and to some extent in Foster and Ling (36). Our stimulus was instead intended to maximize perceptual suppression from the high-contrast surround presentation. Related to the use of adaptation to achieve saturating nonlinearities at the voxel level is the possibility of nonlinear interactions between contrast adaptation or contrast level and surround orientation. Such interactions could result in changes in CRF shape not captured by Nakaruston modeling. There is some support for these interactions in our data; specifically, in area V1, the BOLD responses to low contrasts (below the adaptor contrast, between 4% and 8%) show larger divergence whereby the collinear responses are reduced further, especially closest to the boundary. This is consistent with our general finding that BOLD signal reduction by collinear surround is most pronounced close to the boundary. To determine whether the divergent effects are due to contrast adaptation, scans without the contrast adaptation would have to be conducted. However, varied interactions between center contrast and surround orientation have been reported in the literature (7, 51).

A suggested purpose of feature-dependent surround suppression is to serve texture segmentation (12, 19, 52–54), and both differences in contrast and orientation signal the presence of areas of higher interest in a visual scene possibly containing borders between objects or textures. Suppressing signals from similar regions and enhancing signals from bordering regions with different textures is thought to achieve higher efficiency in transmitting information via visuocortical spikes (53, 54). Our results suggest this modulation is spatially local at the level of the early visual cortex, which comes as something of a surprise given that the perceptual effect of such center-surround configurations is that of a wholesale attenuation in perceived contrast.

DATA AVAILABILITY

Source data for this study are available at the following DOI: <https://doi.org/10.17605/OSF.IO/6Z5J2>.

ACKNOWLEDGMENTS

We thank the members of the Ling Lab for providing helpful feedback and comments on this work and for their assistance in MRI data collection.

GRANTS

This work was funded by NIH Grant EY028163 to S. Ling. The equipment used was funded by NSF Major Instrumentation Grant 1625552.

DISCLOSURES

No conflicts of interest, financial or otherwise, are declared by the authors.

AUTHOR CONTRIBUTIONS

M.K., I.M.B., and S.L. conceived and designed research; M.K. performed experiments; M.K. analyzed data; M.K. and S.L. interpreted results of experiments; M.K. prepared figures; M.K. drafted manuscript; M.K., I.M.B., and S.L. edited and revised manuscript; M.K., I.M.B., and S.L. approved final version of manuscript.

REFERENCES

1. Cannon MW, Fullenkamp SC. Spatial interactions in apparent contrast: inhibitory effects among grating patterns of different spatial frequencies, spatial positions and orientations. *Vision Res* 31: 1985–1998, 1991. doi:[10.1016/0042-6989\(91\)90193-9](https://doi.org/10.1016/0042-6989(91)90193-9).
2. Xing J, Heeger DJ. Center-surround interactions in foveal and peripheral vision. *Vision Res* 40: 3065–3072, 2000. doi:[10.1016/S0042-6989\(00\)00152-8](https://doi.org/10.1016/S0042-6989(00)00152-8).
3. Zenger-Landolt B, Heeger DJ. Response suppression in V1 agrees with psychophysics of surround masking. *J Neurosci* 23: 6884–6893, 2003. doi:[10.1523/JNEUROSCI.23-17-06884.2003](https://doi.org/10.1523/JNEUROSCI.23-17-06884.2003).
4. Carandini M, Heeger DJ, Movshon JA. Linearity and normalization in simple cells of the macaque primary visual cortex. *J Neurosci* 17: 8621–8644, 1997. doi:[10.1523/JNEUROSCI.17-21-08621.1997](https://doi.org/10.1523/JNEUROSCI.17-21-08621.1997).
5. Cavanaugh JR, Bair W, Movshon JA. Nature and interaction of signals from the receptive field center and surround in macaque V1 neurons. *J Neurophysiol* 88: 2530–2546, 2002. doi:[10.1152/jn.00692.2001](https://doi.org/10.1152/jn.00692.2001).
6. DeAngelis GC, Freeman RD, Ohzawa I. Length and width tuning of neurons in the cat's primary visual cortex. *J Neurophysiol* 71: 347–374, 1994. doi:[10.1152/jn.1994.71.1.347](https://doi.org/10.1152/jn.1994.71.1.347).
7. Polat U, Mizobe K, Pettet MW, Kasamatsu T, Norcia AM. Collinear stimuli regulate visual responses depending on cell's contrast threshold. *Nature* 391: 580–584, 1998. doi:[10.1038/35372](https://doi.org/10.1038/35372).
8. Sengpiel F, Baddeley RJ, Freeman TCB, Harrad R, Blakemore C. Different mechanisms underlie three inhibitory phenomena in cat area 17. *Vision Res* 38: 2067–2080, 1998. doi:[10.1016/S0042-6989\(97\)00413-6](https://doi.org/10.1016/S0042-6989(97)00413-6).
9. Webb BS, Tinsley CJ, Barracough NE, Parker A, Derrington AM. Gain control from beyond the classical receptive field in primate primary visual cortex. *Vis Neurosci* 20: 221–230, 2003. doi:[10.1017/S0952523803203011](https://doi.org/10.1017/S0952523803203011).
10. Webb BS, Dhruv NT, Solomon S, Tailby C, Lennie P. Early and late mechanisms of surround suppression in striate cortex of macaque. *J Neurosci* 25: 11666–11675, 2005. doi:[10.1523/JNEUROSCI.3414-05.2005](https://doi.org/10.1523/JNEUROSCI.3414-05.2005).
11. Chen C-C, Kasamatsu T, Polat U, Norcia AM. Contrast response characteristics of long-range lateral interactions in cat striate cortex. *Neuroreport* 12: 655–661, 2001. doi:[10.1097/00001756-20010326-00008](https://doi.org/10.1097/00001756-20010326-00008).
12. Angelucci A, Bijanzadeh M, Nurminen L, Federer F, Merlin S, Bressloff PC. Circuits and mechanisms for surround modulation in visual cortex. *Annu Rev Neurosci* 40: 425–451, 2017. doi:[10.1146/annurev-neuro-072116-031418](https://doi.org/10.1146/annurev-neuro-072116-031418).

13. Sceniak MP, Ringach DL, Hawken MJ, Shapley R. Contrast's effect on spatial summation by macaque V1 neurons. *Nat Neurosci* 2: 733–739, 1999. doi:[10.1038/11197](https://doi.org/10.1038/11197).
14. Klímová M, Bloem IM, Ling S. The specificity of orientation-tuned normalization within human early visual cortex. *J Neurophysiol* 126: 1536–1546, 2021. doi:[10.1152/jn.00203.2021](https://doi.org/10.1152/jn.00203.2021).
15. Klímová M, Bloem IM, Ling S. Attention preserves the selectivity of feature-tuned normalization. *J Neurophysiol* 130: 990–998, 2023. doi:[10.1152/jn.00194.2023](https://doi.org/10.1152/jn.00194.2023).
16. Self MW, Lorteije JAM, Vangeneugden J, van Beest EH, Grigore ME, Levelt CN, Heimel JA, Roelfsema PR. Orientation-tuned surround suppression in mouse visual cortex. *J Neurosci* 34: 9290–9304, 2014. doi:[10.1523/JNEUROSCI.5051-13.2014](https://doi.org/10.1523/JNEUROSCI.5051-13.2014).
17. Chen C-C. Partitioning two components of BOLD activation suppression in flanker effects. *Front Neurosci* 8: 149, 2014. doi:[10.3389/fnins.2014.00149](https://doi.org/10.3389/fnins.2014.00149).
18. Schallmo M-P, Grant AN, Burton PC, Olman CA. The effects of orientation and attention during surround suppression of small image features: a 7 Tesla fMRI study. *J Vis* 16: 19, 2016. doi:[10.1167/16.10.19](https://doi.org/10.1167/16.10.19).
19. Schwartz O, Simoncelli EP. Natural signal statistics and sensory gain control. *Nat Neurosci* 4: 819–825, 2001. doi:[10.1038/90526](https://doi.org/10.1038/90526).
20. Carandini M, Heeger DJ. Normalization as a canonical neural computation. *Nat Rev Neurosci* 13: 51–62, 2011 [Erratum in *Nat Rev Neurosci* 14: 152, 2013]. doi:[10.1038/nrn3136](https://doi.org/10.1038/nrn3136).
21. Fang Z, Bloem IM, Olsson C, Ma WJ, Winawer J. Normalization by orientation-tuned surround in human V1-V3. *PLoS Comput Biol* 19: e1011704, 2023. doi:[10.1371/journal.pcbi.1011704](https://doi.org/10.1371/journal.pcbi.1011704).
22. Wade AR, Rowland J. Early suppressive mechanisms and the negative blood oxygenation level-dependent response in human visual cortex. *J Neurosci* 30: 5008–5019, 2010. doi:[10.1523/JNEUROSCI.6260-09.2010](https://doi.org/10.1523/JNEUROSCI.6260-09.2010).
23. Heeger DJ. Normalization of cell responses in cat striate cortex. *Vis Neurosci* 9: 181–197, 1992. doi:[10.1017/S0952523800009640](https://doi.org/10.1017/S0952523800009640).
24. Albrecht DG, Hamilton DB. Striate cortex of monkey and cat: contrast response function. *J Neurophysiol* 48: 217–237, 1982. doi:[10.1152/jn.1982.48.1.217](https://doi.org/10.1152/jn.1982.48.1.217).
25. Naka KI, Rushton WAH. S-potentials from luminosity units in the retina of fish (Cyprinidae). *J Physiol* 185: 587–599, 1966. doi:[10.1111/j.physiol.1966.sp008003](https://doi.org/10.1111/j.physiol.1966.sp008003).
26. Gardner JL, Sun P, Waggoner RA, Ueno K, Tanaka K, Cheng K. Contrast adaptation and representation in human early visual cortex. *Neuron* 47: 607–620, 2005. doi:[10.1016/j.neuron.2005.07.016](https://doi.org/10.1016/j.neuron.2005.07.016).
27. Vinke LN, Bloem IM, Ling S. Saturating nonlinearities of contrast response in human visual cortex. *J Neurosci* 42: 1292–1302, 2022. doi:[10.1523/JNEUROSCI.0106-21.2021](https://doi.org/10.1523/JNEUROSCI.0106-21.2021).
28. Bloem IM, Ling S. Normalization governs attentional modulation within human visual cortex. *Nat Commun* 10: 5660, 2019. doi:[10.1038/s41467-019-13597-1](https://doi.org/10.1038/s41467-019-13597-1).
29. McDonald JS, Seymour KJ, Schira MM, Spehar B, Clifford CGW. Orientation-specific contextual modulation of the fMRI BOLD response to luminance and chromatic gratings in human visual cortex. *Vision Res* 49: 1397–1405, 2009. doi:[10.1016/j.visres.2008.12.014](https://doi.org/10.1016/j.visres.2008.12.014).
30. Pihlaja M, Henriksson L, James AC, Vanni S. Quantitative multifocal fMRI shows active suppression in human V1. *Hum Brain Mapp* 29: 1001–1014, 2008. doi:[10.1002/hbm.20442](https://doi.org/10.1002/hbm.20442).
31. Williams AL, Singh KD, Smith AT. Surround modulation measured with functional MRI in the human visual cortex. *J Neurophysiol* 89: 525–533, 2003. doi:[10.1152/jn.00048.2002](https://doi.org/10.1152/jn.00048.2002).
32. Phillips DJ, McDougall TJ, Dickinson JE, Badcock DR. Motion direction tuning in centre-surround suppression of contrast. *Vision Res* 179: 85–93, 2021. doi:[10.1016/j.visres.2020.11.001](https://doi.org/10.1016/j.visres.2020.11.001).
33. Poltoratski S, Maier A, Newton AT, Tong F. Figure-ground modulation in the human lateral geniculate nucleus is distinguishable from top-down attention. *Curr Biol* 29: 2051–2057.e3, 2019. doi:[10.1016/j.cub.2019.04.068](https://doi.org/10.1016/j.cub.2019.04.068).
34. Petrov Y, Carandini M, McKee S. Two distinct mechanisms of suppression in human vision. *J Neurosci* 25: 8704–8707, 2005. doi:[10.1523/JNEUROSCI.2871-05.2005](https://doi.org/10.1523/JNEUROSCI.2871-05.2005).
35. Dale AM. Optimal experimental design for event-related fMRI. *Hum Brain Mapp* 8: 109–114, 1999. doi:[10.1002/\(SICI\)1097-0193\(1999\)8:2/3<109::AID-HBM>3.0.CO;2-W](https://doi.org/10.1002/(SICI)1097-0193(1999)8:2/3<109::AID-HBM>3.0.CO;2-W).
36. Foster JJ, Ling S. Feature-based attention multiplicatively scales the fMRI-BOLD contrast-response function. *J Neurosci* 42: 6894–6906, 2022. doi:[10.1523/JNEUROSCI.0513-22.2022](https://doi.org/10.1523/JNEUROSCI.0513-22.2022).
37. Boynton GM, Demb JB, Glover GH, Heeger DJ. Neuronal basis of contrast discrimination. *Vision Res* 39: 257–269, 1999. doi:[10.1016/S0042-6989\(98\)00113-8](https://doi.org/10.1016/S0042-6989(98)00113-8).
38. Ohzawa I, Sclar G, Freeman RD. Contrast gain control in the cat's visual system. *J Neurophysiol* 54: 651–667, 1985. doi:[10.1152/jn.1985.54.3.651](https://doi.org/10.1152/jn.1985.54.3.651).
39. Kay KN, Winawer J, Mezer A, Wandell BA. Compressive spatial summation in human visual cortex. *J Neurophysiol* 110: 481–494, 2013. doi:[10.1152/jn.00105.2013](https://doi.org/10.1152/jn.00105.2013).
40. Andersson JLR, Skare S, Ashburner J. How to correct susceptibility distortions in spin-echo echo-planar images: application to diffusion tensor imaging. *NeuroImage* 20: 870–888, 2003. doi:[10.1016/S1053-8119\(03\)00336-7](https://doi.org/10.1016/S1053-8119(03)00336-7).
41. Smith SM, Jenkinson M, Woolrich MW, Beckmann CF, Behrens TE, Johansen-Berg H, Bannister PR, De Luca M, Dobrajnik I, Flitney DE, Niazy RK, Saunders J, Vickers J, Zhang Y, De Stefano N, Brady JM, Matthews PM. Advances in functional and structural MR image analysis and implementation as FSL. *NeuroImage* 23, Suppl 1: S208–S219, 2004. doi:[10.1016/j.neuroimage.2004.07.051](https://doi.org/10.1016/j.neuroimage.2004.07.051).
42. Fischl B. FreeSurfer. *NeuroImage* 62: 774–781, 2012. doi:[10.1016/j.neuroimage.2012.01.021](https://doi.org/10.1016/j.neuroimage.2012.01.021).
43. Greve DN, Fischl B. Accurate and robust brain image alignment using boundary-based registration. *NeuroImage* 48: 63–72, 2009. doi:[10.1016/j.neuroimage.2009.06.060](https://doi.org/10.1016/j.neuroimage.2009.06.060).
44. Reuter M, Rosas HD, Fischl B. Highly accurate inverse consistent registration: a robust approach. *NeuroImage* 53: 1181–1196, 2010. doi:[10.1016/j.neuroimage.2010.07.020](https://doi.org/10.1016/j.neuroimage.2010.07.020).
45. Tolhurst DJ, Heeger DJ. Comparison of contrast-normalization and threshold models of the responses of simple cells in cat striate cortex. *Vis Neurosci* 14: 293–309, 1997. doi:[10.1017/S0952523800011433](https://doi.org/10.1017/S0952523800011433).
46. Solomon JA, Sperling G, Chubb C. The lateral inhibition of perceived contrast is indifferent to on-center/off-center segregation, but specific to orientation. *Vision Res* 33: 2671–2683, 1993. doi:[10.1016/0042-6989\(93\)90227-N](https://doi.org/10.1016/0042-6989(93)90227-N).
47. Poltoratski S, Tong F. Resolving the spatial profile of figure enhancement in human V1 through population receptive field modeling. *J Neurosci* 40: 3292–3303, 2020. doi:[10.1523/JNEUROSCI.2377-19.2020](https://doi.org/10.1523/JNEUROSCI.2377-19.2020).
48. Snowden RJ, Hammett ST. The effects of surround contrast on contrast thresholds, perceived contrast and contrast discrimination. *Vision Res* 38: 1935–1945, 1998. doi:[10.1016/S0042-6989\(97\)00379-9](https://doi.org/10.1016/S0042-6989(97)00379-9).
49. Henry CA, Jazayeri M, Shapley RM, Hawken MJ. Distinct spatiotemporal mechanisms underlie extra-classical receptive field modulation in macaque V1 microcircuits. *eLife* 9: e54264, 2020. doi:[10.7554/eLife.54264](https://doi.org/10.7554/eLife.54264).
50. Yu H, Xu F, Hu X, Tu Y, Zhang Q, Ye Z, Hua T. Mechanisms of surround suppression effect on the contrast sensitivity of V1 neurons in cats. *Neural Plast* 2022: 5677655, 2022. doi:[10.1155/2022/5677655](https://doi.org/10.1155/2022/5677655).
51. Toth LJ, Rao SC, Kim DS, Somers D, Sur M. Subthreshold facilitation and suppression in primary visual cortex revealed by intrinsic signal imaging. *Proc Natl Acad Sci USA* 93: 9869–9874, 1996. doi:[10.1073/pnas.93.18.9869](https://doi.org/10.1073/pnas.93.18.9869).
52. Knierim JJ, Van Essen DC. Neuronal responses to static texture patterns in area V1 of the alert macaque monkey. *J Neurophysiol* 67: 961–980, 1992. doi:[10.1152/jn.1992.67.4.961](https://doi.org/10.1152/jn.1992.67.4.961).
53. Müller JR, Metha AB, Krauskopf J, Lennie P. Local signals from beyond the receptive fields of striate cortical neurons. *J Neurophysiol* 90: 822–831, 2003. doi:[10.1152/jn.00005.2003](https://doi.org/10.1152/jn.00005.2003).
54. Levitt JB, Lund JS. Contrast dependence of contextual effects in primate visual cortex. *Nature* 387: 73–76, 1997. doi:[10.1038/387073a0](https://doi.org/10.1038/387073a0).